View metadata, citation and similar papers at core.ac.uk

brought to you by CORE

provided by Digital Repository @ Iowa State University

IOWA STATE UNIVERSITY
Digital Repository

Chemistry Publications | Chemistry

2005

Elastic and inelastic deformations of ethylene-passivated tenfold decagonal Al-Ni-Co quasicrystal surfaces

Jeong Young Park
Lawrence Berkeley National Laboratory

D. F. Ogletree
Lawrence Berkeley National Laboratory

M. Salmeron
Lawrence Berkeley National Laboratory

R. A. Ribeiro
Iowa State University

Paul C. Canfield
Iowa State University, canfield@ameslab.gov

See next page for additional authors

Follow this and additional works at: http://lib.dr.iastate.edu/chem_pubs

Part of the Biological and Chemical Physics Commons, Materials Science and Engineering Commons, and the Physical Chemistry Commons

The complete bibliographic information for this item can be found at http://lib.dr.iastate.edu/chem_pubs/46. For information on how to cite this item, please visit http://lib.dr.iastate.edu/howtocite.html.

This Article is brought to you for free and open access by the Chemistry at Digital Repository @ Iowa State University. It has been accepted for inclusion in Chemistry Publications by an authorized administrator of Digital Repository @ Iowa State University. For more information, please contact digirep@iastate.edu.

Authors
Jeong Young Park, D. F. Ogletree, M. Salmeron, R. A. Ribeiro, Paul C. Canfield, Cynthia J. Jenks, and Patricia A. Thiel

This article is available at Digital Repository @ Iowa State University: http://lib.dr.iastate.edu/chem_pubs/46

Elastic and inelastic deformations of ethylene-passivated tenfold decagonal Al-Ni-Co quasicrystal surfaces

Jeong Young Park, D. F. Ogletree, and M. Salmeron*
Materials Sciences Division, Lawrence Berkeley National Laboratory, University of California, Berkeley, California 94720

R. A. Ribeiro and P. C. Canfield
Ames Laboratory and Department of Physics and Astronomy, Iowa State University, Ames, Iowa 50011

C. J. Jenks and P. A. Thiel
Ames Laboratory and Department of Chemistry, Iowa State University, Ames, Iowa 50011
(Received 10 June 2004; revised manuscript received 14 September 2004; published 19 April 2005; corrected 21 April 2005)

The adhesion and friction force properties between a tenfold Al-Ni-Co decagonal quasicrystal and a titanium nitride (TiN)-coated tip were investigated using an atomic force microscope in ultrahigh vacuum. To suppress the strong chemical adhesion found in the clean quasicrystal surfaces, the sample was exposed to ethylene that formed a protective passivating layer. We show that the deformation mechanism of the tip-substrate junction changes from elastic to inelastic at a threshold pressure of 3.8 to 4.0 GPa. Images of the indentation marks left above the threshold pressure indicate the absence of new steps, and indicate that surface damage is not accompanied by formation of slippage planes or dislocations, as found in plastically deforming crystalline materials. This is consistent with the lack of translational periodicity of quasicrystals. The work of adhesion in the inelastic regime is five times larger than in the elastic one, plausibly as a result of the displacement of the passivating layer. In the elastic regime, the friction dependence on load is accurately described by the Derjaguin-Müller-Toporov (DMT) model, consistent with the high hardness of both the TiN tip and the quasicrystal sample. Above the threshold pressure, the friction versus load curve deviates from the DMT model, indicating that chemical bond formation and rupture contribute to the energy dissipation.

DOI: 10.1103/PhysRevB.71.144203 PACS number(s): 61.44.Br, 62.20.Fe, 62.20.Qp, 68.37.Ef

I. INTRODUCTION

At high loads, the friction and adhesion between two contacting solid surfaces are often accompanied by wear as a result of irreversible deformation of the bodies. This deformation is of plastic or brittle character depending on the material. At sufficiently low load, friction and adhesion phenomena can occur in the absence of irreversible deformations in the bulk, near the surface region, i.e., under conditions where only elastic deformation occurs. It is of considerable interest to understand the crossover between the regimes of elastic and inelastic deformation, and the ways that information obtained in one regime can be applied to the other. However, to avoid masking these effects by the occurrence of strong chemical bonds at the interface, which always takes place when clean and chemically active surfaces come into contact, it is necessary to chemically passivate the interface. In this paper we present an experimental study that probes the changes in nanoscale structure and behavior of the contacting surfaces, and the applicability of contact mechanics models in the regimes of elastic and inelastic deformation. Atomic force microscopy (AFM) is particularly suited for this investigation, since it makes possible both the measurement of tribological properties and surface visualization at the nanometer scale.[1–4] One can thus detect the onset of surface damage—inelastic deformation—with atomic-scale precision.[5–8]

Previous experiments with well characterized surfaces carried out in ultrahigh vacuum (UHV) have shown that the relation between friction force and contact area can be described by the Derjaguin-Müller-Toporov[3,9] (DMT) or the Johnson-Kendall-Roberts (JKR) model,[10,11] depending on the adhesion energy and on the hardness of the contacting materials. These two models have been developed as approximations for the elastic behavior in two opposite extremes, one for soft and adhesive materials, and the other for hard and poorly adhesive ones. Any real situation is, of course, intermediate between these two extremes.[12,13] To decide whether the behavior will be closer to that predicted by DMT or JKR, an empirical nondimensional Tabor parameter $\tau = (16R\gamma^2/9K^2z_0^3)^{1/3}$,[14] is found to be appropriate. In this formula, R is the tip radius, γ is the work of adhesion, z_0 is the equilibrium spacing of two surfaces (roughly an atomic distance), and K is the combined elastic modulus of the two materials, given by $K=(4/3)[(1-\nu_1^2)/E_1+(1-\nu_2^2)/E_2]^{-1}$, where E_1 and E_2 are their Young moduli and ν_1 and ν_2 are the Poisson ratios. Empirically, it is found that the JKR model is a good approximation when $\tau>5$, while the DMT is more appropriate when τ is less than 0.1.

A quasicrystal surface was chosen for investigation. Tribological properties are of particular interest in quasicrystals, materials with atoms arranged in patterns with rotational symmetry but no translational periodicity,[15] because low coefficients of friction and low adhesion to polar liquids have been reported for surfaces in air[16–19] and also in vacuum studies.[20–23] The relationship between these anomalous surface properties and the surface atomic structure, however, is unclear. One basic issue is the relative importance of elastic

 ©2005 The American Physical Society

versus inelastic deformation processes to the relatively low friction coefficient, because of the high intrinsic hardness of quasicrystals. The present study is a necessary step toward addressing that issue, as it clearly reveals experimental conditions under which the elastic and inelastic regimes can be separated by use of chemical passivation, thus facilitating measurement of friction forces without perturbation of the quasicrystalline atomic structure.

In previous work[23] we have shown that contacts between W_2C-coated AFM tips and the clean surface of a decagonal quasicrystal, Al-Ni-Co, were strongly adhesive, giving rise to pull-off forces as large as 1.0 μN. This large adhesion produced damage to the quasicrystal surface as a result of rupturing strong chemical bonds formed upon contact, thus making it impossible to probe the clean surface without inelastic deformation. In this study a passivation strategy was implemented, consisting of the chemisorption of a small hydrocarbon molecule, ethylene. Ethylene is expected to saturate after formation of a chemisorbed layer, which produces a relatively small perturbation to the atomic structure of the substrate. This passivation strategy successfully allowed us to probe adhesion and friction either in the elastic regime, or in the inelastic regime, depending on applied load.

II. EXPERIMENT

Sample preparation and characterization were performed in a UHV chamber with a base pressure of 1.0×10^{-10} Torr. The UHV atomic force microscopy system consists of a commercial RHK AFM unit mounted on a 6 in. flange. The sample can be transferred from the AFM head to a manipulator in another area of the chamber for surface preparation and characterization. Heating was accomplished by electron-beam bombardment, Ar^+ ion sputtering was used for sample cleaning, and low-energy electron diffraction (LEED)/Auger electron spectroscopy for surface analysis.[23] Samples and cantilevers could be transferred from air through a load-lock without breaking vacuum, thus allowing convenient exchange of cantilevers with different spring constants and coatings. By using conductive cantilevers, the current between the tip and the sample could be measured and used for feedback control in the scanning tunneling microscopy (STM) mode. Alternatively or simultaneously, the bending of the cantilever was used to determine the interaction force between tip and surface. For normal load calibration we used the spring constant value provided by the manufacturer. Lateral forces were calibrated by the method described in Ref. 24. We used cantilevers coated with approximately 20–30 nm of TiN, with spring constants of 3.0 N/m for contact mode or 48 N/m for tunneling mode. The high stiffness of the latter cantilevers suppresses the jump to contact instability found with soft cantilevers, thus ensuring stable tunneling. With a field-emission scanning electron microscope, the radius of the metal-coated cantilever was found to be 30–50 nm before contact with the surface. After contact, the radius was measured to be 80–120 nm. Since the measured friction force does not change while at constant load and does not show time-dependent behavior in the elastic regime, it is fair to assume that the changes in tip radius took place right after the first contact, with no subsequent changes during contact measurement.

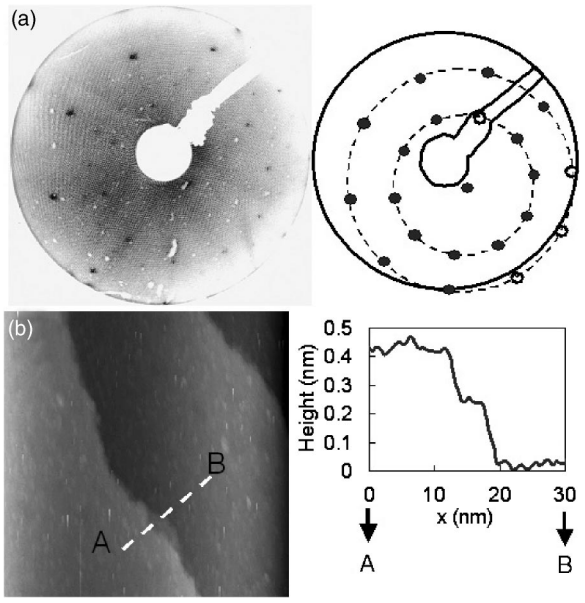

FIG. 1. (a) A LEED pattern of the clean surface at an electron energy of 75 eV. The inset is a schematic representation of the LEED pattern, showing two rings of tenfold spots and satellite spots in-between. (b) 100 nm$\times$100 nm STM image of a tenfold decagonal Al-Ni-Co quasicrystal surface (V_s=1.0 V, I=0.1 nA). Height profile in the inset along the line between A and B shows the terraces with average width of 50–100 nm separated by single steps 0.2 nm high.

The tenfold decagonal sample had dimensions of 1 cm $\times$1 cm$\times$1.5 mm and was cut from a large single grain $Al_{72.4}Ni_{10.4}Co_{17.2}$ quasicrystal grown at the Ames Laboratory, in Iowa State University. The chemical composition was determined by energy dispersive x-ray analysis in a scanning electron microscope. After degreasing by ultrasonic agitation in acetone and methyl alcohol, the sample was introduced into the UHV chamber. The *in situ* cleaning process consists of cycles of Ar^+ ion beam sputtering with 1 keV ion energy, followed by heating for 1–2 h at a temperature up to 1150 K. After cooling, the sample was characterized by LEED/Auger electron spectroscopy and transferred to the sample stage for AFM/STM measurement.

III. RESULTS

A. Preparation and passivation of the quasicrystal surface

Earlier studies of tenfold decagonal Al-Ni-Co quasicrystals[25,26] indicate that the structure consists of two types of atomic layers stacked in an alternating sequence along the tenfold direction with an interlayer spacing of 0.204 nm. Each layer has local pentagonal symmetry, and neighboring layers are related by inversion symmetry. Figure 1(a) shows a LEED pattern of the clean surface acquired at an electron energy of 75 eV. The inset in the right is a schematic representation of the LEED pattern, which consists of two rings of spots arranged with tenfold symmetry and con-

taining satellite spots in between. The ratio of the radii of the two concentric rings is 1.63, close to the expected value of the Golden Mean $(1+5^{1/2})/2=1.618$, within the error of measurement.

Figure 1(b) shows a 100 nm$\times$100 nm STM image of the clean surface taken with a sample bias of 1 V and tunneling current of 0.1 nA. A TiN-coated cantilever with a spring constant of 48 N/m was used. As shown by line profiles across steps in the inset, the height of single and double steps are 0.20 nm and 0.41 nm, respectively. The surface corrugation on the terrace is less than 0.02 nm and the terrace average width is 50–100 nm.

Ethylene exposure was performed by backfilling the chamber to a pressure of 4.0×10^{-7} Torr at room temperature. After a 20 L exposure, the LEED pattern disappeared completely, suggesting that no ordered superstructures are formed after ethylene adsorption. The ethylene exposure required to cause the disappearance of the pentagonal diffraction pattern (20 L) is twice as large as that found when using oxygen (10 L) in our previous experiments.[23] The carbon uptake from ethylene adsorption was monitored by Auger spectroscopy. The peak-to-peak ratio of the carbon 252 eV peak to the Al 68 eV peak reached a value of 5 after 100 L exposure and remained constant thereafter, indicating that adsorption of ethylene saturated at 100 L.

B. Confirmation of passivation

On the clean surface we obtain a tip-sample adhesion force of 530±100 nN, using the value of 3.0 N/m for the spring constant provided by the manufacturer. A 30% uncertainty is estimated for this value of the spring constant. The 100 nN error is the standard deviation of multiple measurements of the force-distance curves. This large error reflects possible changes in radius and chemical composition. The adhesion force of 530 nN is about half the 1.02 μN value found previously with TiN-coated tips on stiffer levers (48 N/m), and two thirds of the 850 nN value found with W_2C-coated tips on 11.5 N/m cantilevers.[23] Again, this variation is likely associated with differences in tip radius and cleanliness, as well as the uncertainties in the spring constant value.

After a 300 L exposure of ethylene at room temperature, the adhesion force was reduced to a value of 13±2 nN; i.e., about two orders of magnitude smaller. Images acquired after these contact experiments revealed that the surface topography remained unchanged within the angstrom scale. Thus, ethylene adsorption made it possible to perform reproducible contact experiments at low loads. All data reported in the remainder of this paper were obtained after ethylene passivation.

C. Elastic and inelastic deformation

Experiments as a function of load show that the surface topography is unmodified up to loads of 600 nN, corresponding to an estimated pressure of 3.8 GPa. The pressure was calculated using the contact area (A) given by the DMT model:[3,12]

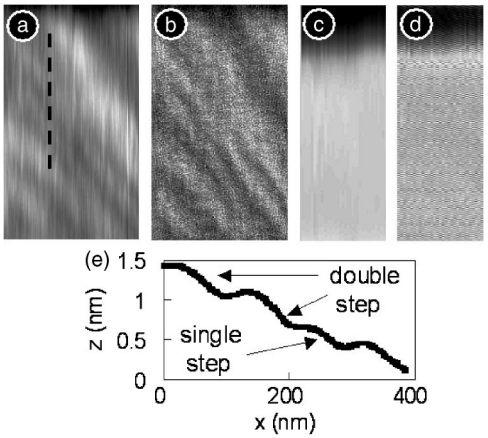

FIG. 2. (a) 500 nm$\times$290 nm contact mode topographic and (b) friction images acquired with an applied load of 400 nN. (c) 500 nm$\times$200 nm topographic and (d) friction images at a load of 750 nN. (e) Height profile through the broken line in (a). The step height and width of terraces is similar as that observed with STM although the resolution is lower. In (c) and (d), the images show the effect of stick-slip, producing the dark bands at the beginning of the scan (top), suggesting that at this higher load the chemical nature of the tip-sample contact has been changed.

$$A=\pi\left(\frac{R^{2/3}}{K^{2/3}}\right)(L+L_c)^{2/3},$$

where L_c is the adhesion force. Using $L_c=13$ nN, $R=100$ nm, and a combined elastic modulus (K) of 171 GPa, [$E_{TiN}=600$ GPa, $E_{QC}=200$ GPa, $\nu_{TiN}=0.25$, $\nu_{QC}=0.38$ (see Ref. 27)] we find $A=158$ nm^2. The P (pressure) is then easily calculated as F_n (applied load)/A=600 nN/158 nm^2 =3.8 GPa.

Figure 2 shows contact mode images at increasing loads: (a) topography and (b) friction at a load of 400 nN, and (c) topography and (d) friction at 750 nN. In comparison with the STM mode images [Fig. 1(b)], the AFM resolution is lower, since it is limited by the tip radius of ~100 nm, as shown in the line profile of Fig. 2(e). The step heights, however, are the same in STM and AFM images, with single steps 0.21±0.03 nm high and double steps 0.41±0.04 nm high.

When the load reached 750 nN, corresponding to 4.1 GPa, damage finally occurred, with the tip exhibiting strong static friction, which produced the dark bands in the images at the start of the scan in Figs. 2(c) and 2(d). The stick-slip due to the strong increase in adhesion and the resulting damage prevented reproducible imaging at this point. This was confirmed by subsequently scanning a larger area (0.95 μm$\times$1.0 μm), which included the area in Fig. 2. Figures 3(a) and 3(b) are topographic and friction AFM images acquired at a load of 150 nN. The surface shows a trench in the previously scanned area with a depth of 1.0±0.2 nm, and a width of approximately 500 nm$\times$200 nm with debris accumulated at the edges. The volume of the hole is ~3 $\times10^5$ nm^3, approximately equal to that of the mounds within

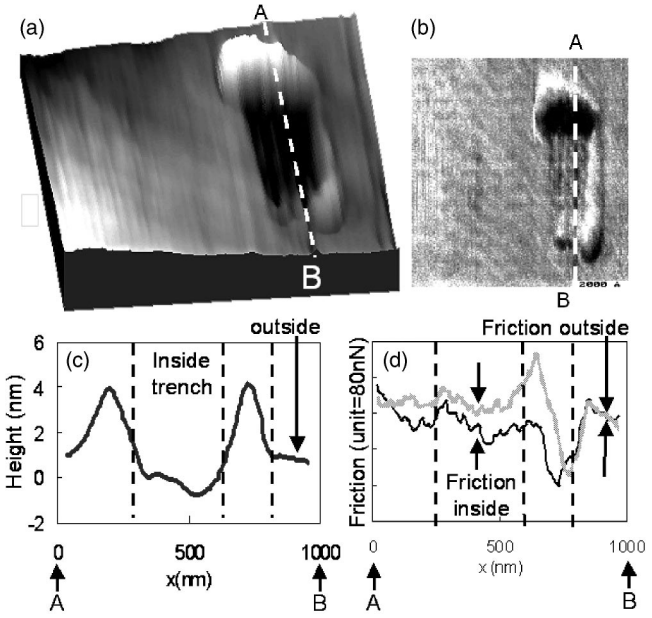

FIG. 3. (a) 0.95 μm $\times$ 1.0 μm topographic AFM image and corresponding friction images (b), acquired at an applied load of 150 nN. A central area, previously scanned with a load of 750 nN (corresponding to a pressure of 4.1 GPa), is inelastically deformed, showing a trench with a depth of 1.0 nm, and debris at the edge. Height (c) and friction (d) profiles across the trench show that the friction force inside the trench is 74 nN $\pm$ 13 nN, higher than that of outside (14 nN $\pm$ 4 nN) by a factor of 5.

the error of AFM imaging. Since the image resolution did not change, we can assume that there is little damage in the tip and that most of the damage occurred in the sample side of the junction.

Topographic and friction line profiles are also shown in Figs. 3(c) and 3(d). The friction profiles in the two scanning directions show that the friction force (gap between two friction curves) inside the trench is 74 nN $\pm$ 13 nN, higher than that of outside (14 nN $\pm$ 4 nN) by a factor of 5. This result can be explained by assuming that some of the protective hydrocarbon layer has been removed and that the clean surface is exposed in the deformed region.

Another interesting observation is the unmodified step structure of the surface, which was only interrupted by the trench. No additional steps were created by the deformation, indicating that no dislocation or slippage planes have been created. This is in contrast to the case of nanoindentation experiments with gold single crystals, where new steps or dislocations were created by emerging slippage planes,[28,29] as expected in plastic deformation processes. The damage in our quasicrystals is therefore of a brittle nature, mostly due to rupture of localized metal–metal bonds.

D. Indentation experiments

Figure 4 shows a plot of adhesion force as a function of maximum applied load. In the elastic regime, which extends up to loads of 600 nN, the adhesion force is constant at 13 $\pm$ 2.0 nN. Adhesion increases rapidly to 70 $\pm$ 9.0 nN upon crossing the threshold for plastic deformation near 700 nN.

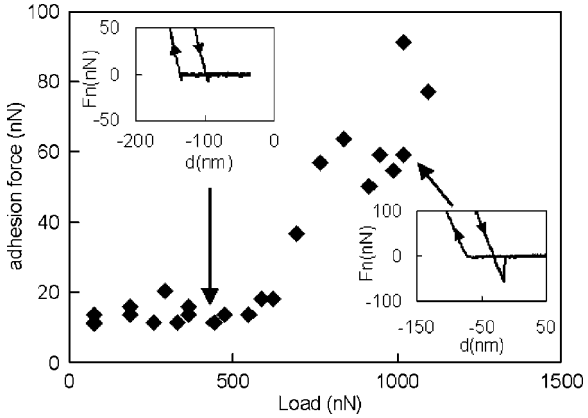

FIG. 4. Plot of adhesion force as a function of applied load. In the elastic regime, up to an applied load of 600 nN, the adhesion force is 13 nN. It increased up to 70 nN in the inelastic regime. Two force-distance curves, corresponding to these two regimes are shown in insets.

Two representative force-distance curves in these two regimes are shown as insets. We interpret the increase in adhesion force in the inelastic regime as a result of the formation of chemical bonds between the tip and the surface due to the displacement of protective hydrocarbon molecules. The adhesion force of 70 nN is, however, still much smaller than that measured on the clean surface (530 nN), suggesting that only a fraction of the passivating molecules have been removed.

E. Friction versus load experiments

Figure 5 shows friction versus load measurements between a TiN-coated cantilever and the passivated quasicrystal surface. DMT and JKR fittings satisfying the condition of

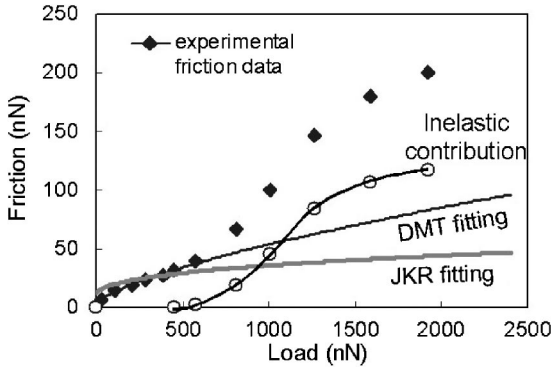

FIG. 5. Plot of the friction force as a function of applied load. The lines are DMT and JKR fittings using the constraint of an adhesion force (L_c) of 13 nN. The DMT curve fits very well with the experimental data in the elastic regime, consistent with contact of two hard materials, TiN and the passivated quasicrystal. Open circles represents the inelastic contribution to the friction force and energy dissipation, which is the difference between the experimental friction and the extrapolated DMT values.

13 nN adhesion force are shown for comparison. It is clear that the DMT fit is in good agreement with the experimental data in the elastic regime and consistent with the fact that the two contacting materials, TiN and quasicrystal, are very hard. The Tabor parameter, using a tip radius of 100 nm, $z_0 = 2$ Å, is $\tau = 0.056$, effectively indicating that the DMT model is the appropriate model for this case. The DMT fit provides a value for the work of adhesion of 20.7 mJ/m^2 and an elastic shear stress of 243 MPa.

The rapid increase in friction force above 600 nN is clearly related to the inelastic processes resulting from bond formation and rupture. The contribution of these processes to friction dissipation is given by the difference between the experimental curve and the DMT fitting above 600 nN, as shown in the figure by the open circles.

IV. DISCUSSION

We have seen that the transition from elastic to inelastic deformation occurs rather abruptly at 3.8 to 4.0 GPa. The absolute value of transition pressure, however, has a significant error bar ($\sim$50%), due partially to uncertainties of spring constant ($>$30%), and partially to the scattering of multiple measurements with different tips ($\sim$20%).

The transition in the nature of the mechanical contact produces two related changes in the tribological properties. One is the change in adhesion energy from a constant value in the elastic regime, to a value in the inelastic regime that is about five times higher. Second, the friction force, which is well described by the DMT model in the elastic regime, cannot be extrapolated to the inelastic regime. In other words, there is a concomitant change in the shear stress, from a constant value in the elastic regime to a high and variable value in the inelastic regime. We anticipate that these two differences in tribological properties will be qualitatively observed on other passivated metal surfaces, upon crossing between elastic and inelastic regimes, and are not unique to the quasicrystal—although, of course, the quantitative aspects, such as the transition pressure, will depend both upon the tip and the surface.

It is interesting to notice that the DMT model developed for elastic deformation of hard and poorly adhesive materials (a condition satisfied by our tip and surface materials), applies well below 3.8 GPa, while the same two materials follow the JKR model in the absence of a passivating layer. This is mainly because the high adhesion force in the absence of such layer is sufficient to change the Tabor parameter from a low value (<0.1) to a high value above 5.[23]

It is worthwhile to mention that our tip-sample mechanical contact shows an intermediate regime at applied loads between 600 and 700 nN, with both elastic and inelastic contributions. We observed a time-dependent change of friction force in this regime, which may be associated with the accumulation of atomic defects in the contact.[30] The abruptness in the elastic to inelastic response in a quasicrystal has also been observed in previous nanoindentation experiments.[31] It was attributed to a local transformation to a crystalline phase in the quasicrystal,[32] which has also been observed in friction experiments.

In our quasicrystalline material surface damage was not accompanied by formation of slippage planes or dislocations, as observed previously on a crystalline surface such as Au,[28,29] where formation of dislocations is a prevalent mechanism of plastic deformation. In the quasicrystals, however, the lack of translational symmetry prevents the formation of easy slippage planes and is likely one of the reasons for the high hardness of these materials. Because of the lack of evidence of concerted motion, we attribute the damage observed here to localized bond rupture, giving rise to atomic scale wear. The present results are fully in line with this mechanism.

Another AFM study of adhesion forces on a clean metal surface, namely, on Pt(111), has been reported previously,[33] although such studies of nonmetallic surfaces are much more common. For a W_2C tip and Pt(111), it was also found that the adhesion force was strong—in fact, about an order of magnitude stronger than for the clean quasicrystalline Al-Ni-Co surface. This suggests that the adhesion on the clean quasicrystal, while strong in an absolute sense, may still be weak in comparison with clean transition metals. The strong adhesion on Pt(111) could be circumvented by carbon and oxygen contamination, although the regimes of elastic and inelastic deformation were not delineated as in the present study.

V. CONCLUSIONS

We have investigated the tribological properties of contacts between a TiN-coated tip and an ethylene passivated tenfold Al-Ni-Co quasicrystal. Monolayer passivation allowed us to explore the elastic deformation regime up to loads of 600 nN (or 3.8 GPa) without damaging the tip or the surface. We found that the adhesion remained constant in this regime, but increased by a factor of five after crossing into the inelastic regime. We explained this as due to strong chemical interactions between tip atoms and exposed atoms of the substrate where the passivating hydrocarbon molecules had been displaced. The wear mechanism in the inelastic regime appears to be the result of bond rupture and displacement of substrate atoms. No slippage planes or dislocations were observed to emerge at the surface, as is typically the case in normal crystalline metals.

The friction force is well described by the DMT model in the elastic regime, consistent with the hard nature of TiN and quasicrystal materials. In the inelastic regime, the measured friction force shows a significant departure from the DMT fitting, indicating that chemical bond formation and rupture contribute largely to the energy dissipation.

ACKNOWLEDGMENTS

This work was supported by the Director, Office of Energy Research, Office of Basic Energy Sciences, Materials Sciences Division, of the U.S. Department of Energy through the Ames Laboratory, Contract No. W-405-Eng-82, and through the Lawrence Berkeley National Laboratory, Contract No. DE-AC03-76SF00098.

*Author to whom correspondence should be addressed. Electronic address: salmeron@stm.lbl.gov

[1] E. Gnecco, R. Bennewitz, T. Gyalog, and E. Meyer, J. Phys.: Condens. Matter **13**, R619 (2001).
[2] R. W. Carpick and M. Salmeron, Chem. Rev. (Washington, D.C.) **97**, 1163 (1997).
[3] M. Enachescu, R. J. A. van den Oetelaar, R. W. Carpick, D. F. Ogletree, C. F. J. Flipse, and M. Salmeron, Phys. Rev. Lett. **81**, 1877 (1998).
[4] M. Dienwiebel, G. S. Verhoeven, N. Pradeep, J. W. M. Frenken, J. A. Heimberg, and H. W. Zandbergen, Phys. Rev. Lett. **92**, 126101 (2004).
[5] R. Luthi, E. Meyer, H. Haefke, L. Howald, W. Gutmannsbauer, M. Guggisberg, M. Bammerlin, and H. J. Guntherodt, Surf. Sci. **338**, 247 (1995).
[6] S. G. Corcoran, R. J. Colton, E. T. Lilleodden, and W. W. Gerberich, Phys. Rev. B **55**, R16 057 (1997).
[7] J. Hu, X. D. Xiao, D. F. Ogletree, and M. Salmeron, Surf. Sci. **327**, 358 (1995).
[8] J. Fraxedas, S. Garcia-Manyes, P. Gorostiza, and F. Sanz, Proc. Natl. Acad. Sci. U.S.A. **99**, 5228 (2002).
[9] B. V. Derjaguin, V. M. Muller, and Y. P. Toporov, J. Colloid Interface Sci. **53**, 314 (1975).
[10] K. L. Johnson, K. Kendall, and A. D. Roberts, Proc. R. Soc. London, Ser. A **324**, 301 (1971).
[11] R. W. Carpick, N. Agraït, D. F. Ogletree, and M. Salmeron, J. Vac. Sci. Technol. B **14**, 1289 (1996).
[12] R. W. Carpick, D. F. Ogletree, and M. Salmeron, J. Colloid Interface Sci. **211**, 395 (1999).
[13] U. D. Schwarz, J. Colloid Interface Sci. **261**, 99 (2003).
[14] J. A. Greenwood, Proc. R. Soc. London, Ser. A **453**, 1277 (1997).
[15] D. Shechtman, I. Blech, D. Gratias, and J. W. Cahn, Phys. Rev. Lett. **53**, 1951 (1984).
[16] S. S. Kang, J. M. Dubois, and J. von Stebut, J. Mater. Res. **8**, 2471 (1993).
[17] R. Wittmann, K. Urban, M. Schandl, and E. Hornbogen, J. Mater. Res. **6**, 1165 (1991).
[18] P. J. Pinhero, J. W. Anderegg, D. J. Sordelet, M. F. Besser, and P. A. Thiel, Philos. Mag. B **79**, 91 (1999).
[19] C. J. Jenks and P. A. Thiel, Langmuir **14**, 1392 (1998).
[20] J. S. Ko, A. J. Gellman, C. Jenks, T. Lograsso, and P. A. Thiel, Surf. Sci. **423**, 243 (1999).
[21] C. Mancinelli, C. J. Jenks, P. A. Thiel, and A. J. Gellman, J. Mater. Res. **18**, 1447 (2003).
[22] J. M. Dubois, P. Brunet, W. Costin, and A. Merstallinger, J. Non-Cryst. Solids **334–335**, 475 (2004).
[23] J. Y. Park, D. F. Ogletree, M. Salmeron, C. J. Jenks, and P. A. Thiel, Tribol. Lett. **17**, 629 (2004).
[24] D. F. Ogletree, R. W. Carpick, and M. Salmeron, Rev. Sci. Instrum. **67**, 3298 (1996).
[25] A. Yamamoto, K. Kato, T. Shibuya, and S. Takeuchi, Phys. Rev. Lett. **65**, 1603 (1990).
[26] M. Kishida, Y. Kamimura, R. Tamura, K. Edagawa, S. Takeuchi, T. Sato, Y. Yokoyama, J. Q. Guo, and A. P. Tsai, Phys. Rev. B **65**, 094208 (2002).
[27] The Young's modulus and Poisson's ratio of single grain I-Al-Pd-Mn were used.
[28] E. Carrasco, O. Rodríguez de la Fuente, M. A. González, and J. M. Rojo, Phys. Rev. B **68**, 180102(R) (2003).
[29] J. D. Kiely and J. E. Houston, Phys. Rev. B **57**, 12 588 (1998).
[30] S. Kopta and M. Salmeron, J. Chem. Phys. **113**, 8249 (2000).
[31] S. Dub, N. Novikov, and Y. Milman, Philos. Mag. A **82**, 2162 (2000).
[32] J. S. Wu, V. Brien, P. Brunet, C. Dong, and J. M. Dubois, Philos. Mag. A **80**, 1645 (2000).
[33] M. Enachescu, R. W. Carpick, D. F. Ogletree, and M. Salmeron, J. Appl. Phys. **95**, 7694 (2004).